Nano Today 26 (2019) 164–175

Contents lists available at ScienceDirect

Nano Today

journal homepage: www.elsevier.com/locate/nanotoday

Review

Structure regulation of noble-metal-based nanomaterials at an atomic level

Junjie Mao [a], Jun Li [a], Jiajing Pei [b,c], Yan Liu [a], Dingsheng Wang [b,*], Yadong Li [b]

[a] Center of Single-Atom, Clusters and Nanomaterials (CAN), Key Laboratory of Electrochemical Clean Energy of Anhui Higher Education Institutes, Key Laboratory of Functional Molecular Solids, Ministry of Education, Anhui Key Laboratory of Molecule-Based Materials, College of Chemistry and Materials Science, Anhui Normal University, Wuhu, 241002, China
[b] Department of Chemistry, Tsinghua University, Beijing, 100084, China
[c] State Key Lab of Organic-Inorganic Composites, Beijing University of Chemical Technology, Beijing, 100029, China

ARTICLE INFO

Article history:
Received 1 January 2019
Received in revised form 20 March 2019
Accepted 25 March 2019
Available online 28 March 2019

Keywords:
Atomic level
Catalytic properties
Noble metal nanomaterials
Intermetallic compounds
Well-controlled

ABSTRACT

Controlling the structure of noble-metal-based nanomaterials (NMNs) with precision at an atomic level has received considerable attention in recent years. However, the complexity of synthetic process poses great challenges in the delicate design and fine control of NMNs. In this review, we focus on recent progress made in the chemical synthesis of NMNs at an atomic level, which include surface engineering of NMNs, atomic layer coating of NMNs, metal doping or substitution, and intermetallic compounds. The catalytic properties of well-controlled NMNs are discussed. Finally, the major challenges and opportunities pertaining to the controllable synthesis of NMNs are presented. We believe this brief review provides up-to-date information on the fine tuning of NMNs structures, and offers some new perspectives of this rapidly developing field.

Contents

Introduction

The world is facing serious problems due to rapid consumption of non-renewable resources, shortage of energy resources, and environmental pollution. Development of efficient and clean energy technology has become the top priority of current scientific research. In this context, catalysts, especially noble metal catalysts, play a key role in energy conversion and storage for improving conversion efficiency and selectivity and at the same time cause less environmental pollution [1–9]. For example, nanostructured Au has received consideration attention in electrocatalysis, organic catalysis, sensor and biomedicine field [10–14]. Three-way catalyst, Pt-Pd-Rh with good catalytic performance and anti-toxicity, has been proved the first choice for automotive exhaust gas purification catalysts [15]. Up to now, many research groups have exploited different ways to prepare noble metal nanomaterials (NMNs) with various architectures and compositions, and their catalytic properties have also been investigated [16–46]. It is note-worthy that the alloying of one or two kinds of transition metals with the noble metal has become a valid strategy to develop excellent electrocatalysts. In this regard, many efforts have been made to synthesize

* Corresponding author.
E-mail address: wangdingsheng@mail.tsinghua.edu.cn (D. Wang).

https://doi.org/10.1016/j.nantod.2019.03.008
1748-0132/

multimetallic nanomaterials (MNs). Compared to monometallic nanocrystals, MNs offer more catalytic reaction sites to enable efficient adsorption and activation of substrate molecules or intermediates, thereby, promoting the reaction. Moreover, interactions between different metals regulate the geometric and electronic properties of catalysts showing synergistic effects.

However, understanding the relationship between the fine structure (surface/interface, defect sites, lattice strain, coordination number, etc) and properties of catalysts remains an open challenge. From the structure viewpoint, MNs prepared by conventional chemical methods have poor control and reproducibility, which makes it difficult to determine the structure of active sites. Thus, unclear nanostructures make it impossible to investigate their surface/interface/defect sites/lattice strain-dependent catalytic properties. From the viewpoint of catalytic properties, there remains much room for improvements in catalytic activity and stability of MNs. Usually, nano-sized catalysts without decorations show inferior catalytic activities for oxygen evolution reaction (OER) and oxygen reduction reaction (ORR), resulting in lower overall energy conversion efficiency. As a consequence, design and precise regulation of NMNs structure with high catalytic performance are very important and it requires more efforts on the rational design of microstructures.

The synthesis of well-defined NMNs at atomic level provides an opportunity to solve the afore-mentioned problems. The emergence of some advanced characterization methods, such as aberration-corrected high-angle annular dark-field scanning transmission electron microscopy (HAADF-STEM), X-ray absorption fine structure (XAFS), etc. greatly boosts the developments in this field. For example, XAFS technique can be used to obtain local structure information such as coordination number, bond angle, valence state, and bond length of the catalyst, which helps in the design of nanocatalysts with specific geometries and electronic structures [47,48]. The geometric effects could influence the electronic structure of nanocrystals, changing the catalytic properties. Thus, precisely tuning the geometric structure of nanocrystals is an effective way to boost the catalytic results. In addition, studies have proved that the synthesis of nanomaterials with controlled structures is crucial for achieving desired catalytic properties (activity, selectivity, and stability) [49–52]. Regulation of the microstructure of the catalyst or even changes in several atoms can have significant effects on the catalysis. For example, Yang's group found that ordered AuCu nanocrystals (NCs) could effectively reduce CO_2 to CO [53], while the AuCu alloy with disordered nanostructures mainly produced H_2 during the reduction of CO_2. A similar phenomenon can widely be observed in cases of other nanocatalysts. Although precise synthesis of nanocrystals has been highly successful in recent years, a summary of nanocrystal structure and catalytic reaction at the atomic level has rarely been followed [54]. In this review, we aim to summarize the recent progress on controllable synthesis of NMNs (Fig. 1), which includes surface engineering of NMNs, atomic layer coating of NMNs, metal doping or substitution, intermetallic compounds. More importantly, the above finely regulated structures displayed excellent catalytic properties for ORR, hydrogen evolution reaction (HER), semi-hydrogenation of alkynes, chemoselective hydrogenation, and others. Finally, the challenges and opportunities of controllable synthesis of NMNs at an atomic level are presented.

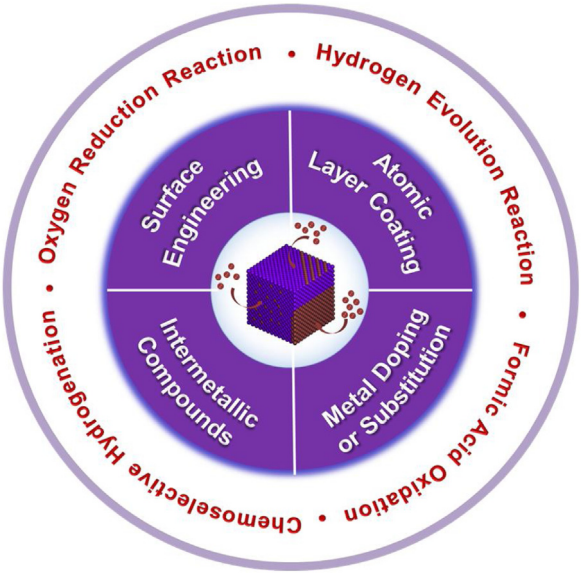

Fig. 1. Schematic illustration showing the fine-tuned structure of NMNs from four perspectives and catalytic applications.

Controllable synthesis of NMNs at an atomic level

Surface engineering

The catalytic properties of metal nanomaterials are strongly related to their surface structures [55–62]. Surface engineering (mainly for post-modification) is an effective strategy for designing catalysts with tailored structures, which constitutes a desirable environment for the catalytic reaction. Generally, the surface engineering strategy allows preparation of nanocrystals with unique morphologies including nanoframe, concave, composition segregated nanostructures, etc. In recent years, a variety of synthetic strategies have been developed to construct specific surface/subsurface with the purpose of elevating the catalytic performance, e.g., chemical etching to cause atomic rearrangement, electrochemical de-alloying to form segregated surfaces, atmosphere annealing to design phase interface, gas-assisted reduction to manufacture defects, et al. Among them, the chemical etching strategy can be managed to selectively remove active metal atoms from alloy nanocrystals to fabricate novel concave/hollow structures by precisely controlling the etching strength and the reaction environment. The remaining atoms of NCs will spontaneously rearrange, leading to the post-decoration on size, shape and composition of NCs. For example, Li et al. developed a controllable coordination-assisted strategy to obtain concave Pt-Ni alloys by using dimethylglyoxime as the corrosion ligand (Fig. 2a–d) [63]. They chose octahedral $PtNi_{10}$ as a model to study the etching evolution mechanism. The concavity increased with the prolonged chemical etching time owing to the larger dissolution rate of Ni soluble species than that of Pt. The initiation of etching process would be accustomed to occuring along {100} direction for transforming the octahedron into spherical particles. It indicated that the etching process was firstly performed at the corner. The etching process gradually transferred from original {100} direction to the {110} and {111} directions when the new narrow {100} facets emerged. During the further etching process, the edges and facets were excavated into the cavities while the metal atoms of pristine octahedral were rearranged to form concave structure. They applied DFT to calculate the cohesive energy regarding the chemical potential of the metal atoms, suggesting that the different etching priorities at specific sites of octahedron were governed by the cohesive energy. Benefiting from the large surface area and high density of exposed atomic steps or defects, the concave $PtNi_3$ nanostructure exhibited superior catalytic activity and stability compared to the uncorroded $PtNi_3$ and Pt_3Ni catalysts.

Additionally, the etchants with different preferential etching capacities can lead to the production of various unexpected struc-

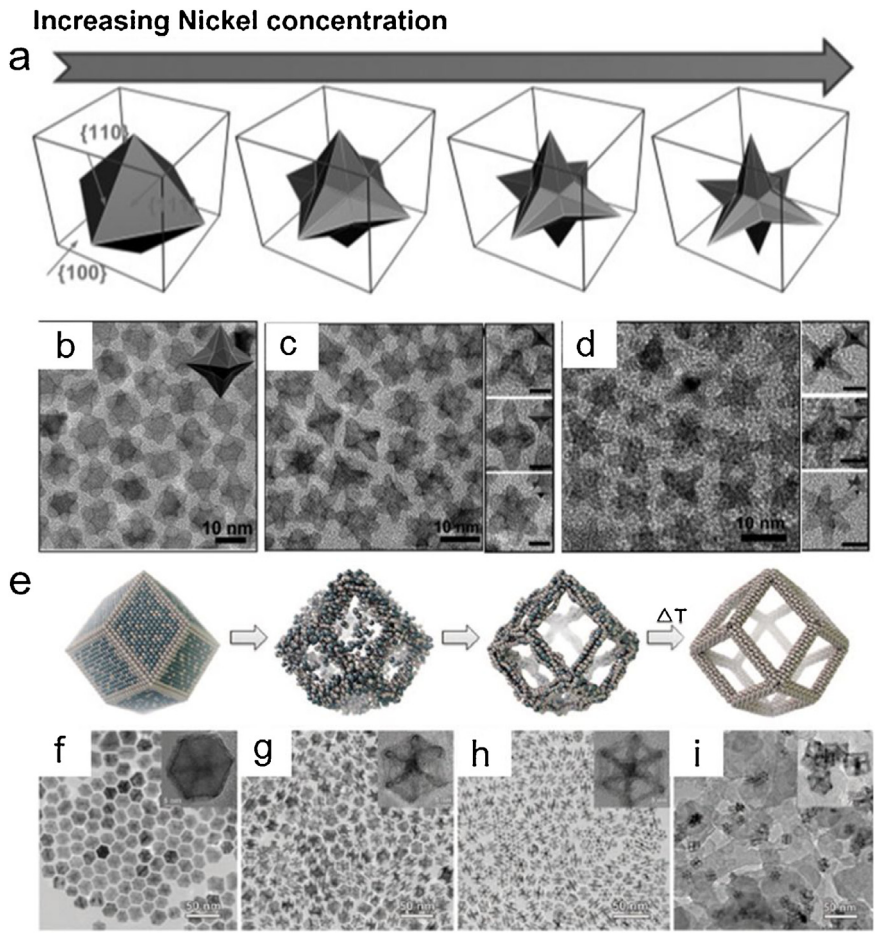

Fig. 2. (a) The evolution of nanoparticle shape as a function of Ni:Pt mole ratio in the Ni-rich alloys, TEM images of corroded (b) $PtNi_2$, (c) $PtNi_3$ and (d) $PtNi_{10}$. Reprinted with permission from Ref. [63]. Copyright 2012, Wiley-VCH. (e) Schematic illustrations of the samples obtained at different stages, TEM images of (f) initial solid Pt_3Ni, (g) PtNi intermediates, (h) Final Pt_3Ni nanoframes, (i) Annealed Pt_3Ni nanoframes dispersed on high surface area carbon. Reprinted with permission from Ref. [64]. Copyright 2014, American Association for the Advancement of Science.

tures (e.g. nanoframe). The nanocage or nanoframe structures with high specific surface area, large void space and good three-dimensional accessibility have attracted a wide attention in recent years. Choosing a suitable etchant is a great challenge for controlling and moderating the corrosion process. Recently, Yang and coworkers reported the highly opened Pt-rich Pt_3Ni nanoframes by selecting oleylamine (OAm) as the corrosion ligand (Fig. 2e–i) [64]. $PtNi_3$ polyhedra were first synthesized in OAm system under Ar atmosphere. The as-prepared OAm-capped $PtNi_3$ rhombic dodecahedra were redispersed in hexanes and finally converted to Pt_3Ni nanoframes under ambient conditions for 2 weeks. OAm plays a critical role in corrosion by readily creating soluble complexes with Ni^{2+}. The nanoframes with 2 nm thick edges could also be fabricated faster via the preferential dissolution of rich Ni species by holding at 120 °C just for 12 h. Furthermore, the surfactant OAm was removed by thermal annealing to make surface-clean nanoframes before electrochemical measurement. The highly opened Pt_3Ni nanoframes with three-dimensional structure greatly enhanced the accessibility of the reactants to both interior and exterior surfaces, which ensured the high catalytic activity and durability for ORR compared with benchmark catalysts. Occasionally, etching and galvanic replacement reaction are occurred simultaneously in one system because of the different electronegativities of multi-metals. Furthermore, Li and coworkers used this feature to prepare Au island on Pt-Ni trimetallic nanoframe catalysts by the combination of priority-related chemical etching and the electronegativity difference between Ni and Au atoms [65]. Chemical etching plays a major role in the formation of frame-work structure. First, the galvanic replacement reaction took place between Au (III) and Ni (0) species owing to the lower electronegativity of Ni. It was estimated that galvanic replacement reaction occupied dominantly in the corner because the Ni with high free energy at low-coordination corner sites was readily oxidized. During the gradual progress of the etching, the Au atoms aggregated into isolated islands at the top of the truncated octahedral $PtNi_3$. The segregated Pt-skin edges with decorated Au island (denoted as 10% Au on Pt_3Ni) showed higher catalytic activity for methanol electrooxidation and 4-nitrobenzaldehyde hydrogenation than the $PtNi_3$ polyhedron and Pt_3Ni bimetallic nanoframes.

However, the chemical etching often occurs in random sites and difficult to control, thus the expected structures may be destroyed during the corrosion process. Removing the active transition metal component of catalysts during the actual catalytic reaction is an effective tactic to form unique surface and promote the catalytic performance. For instance, Duan and coworkers discovered that Ni atoms were removed from one-dimensional PtNi alloy nanowires (NWs) to reach jagged Pt NWs (J-Pt NWs) by electrochemical dealloying process [66]. The J-Pt NWs displayed an ultrahigh mass activity and electrochemical active surface area (ECSA) toward ORR compared with Pt/C and regular Pt NWs (R-Pt NWs). At first, the Pt/NiO core/shell NWs were synthesized by a simple wet chemical method. Then, the as-obtained Pt/NiO NWs supported on conductive carbon black were annealed at 450 °C under a reducing atmosphere (Ar/H_2: 97/3) to form alloy configurations. Finally, the

pure ultrafine J-Pt NWs were achieved via cyclic voltammetry while Ni acted as a sacrificial agent. The DFT simulation revealed that the shorter Pt-Pt bond length was presented at J-Pt NWs than R-Pt NWs and Pt/C, which resulted in a high compressive strain on the rough and undercoordinated Pt-rich surface structures.

Another surface modification method is atmosphere annealing, by which the internal noble metal atoms will be migrated to the surface or near surface. Guo et al. calcined the pre-prepared PtCo Zigzag nanowires (z-NWs) at 400 °C in N_2 atmosphere to acquire high-index faceted Pt-skin PtCo z-NWs [67]. The atomic arrangement on the surface of NWs and the spatial element distribution of near-surface region would be simultaneously controlled at N_2 atmosphere. They proved that Pt-skin PtCo z-NWs with high-index facets could promote activation of reactant molecules, resulting in higher electrocatalytic activity relative to low-index facets. The unique structure of Pt-skin PtCo z-NWs showed excellent catalytic activity toward the electrochemical detection of various molecules (H_2O_2, NH_2NH_2, dopamine, and acetaminophen) and ORR in the acid. Annealing at different atmospheres leads to the formation of different structures. Huang's group designed multiphase interfaces by controlling different annealing atmospheres, and developed Pt-Ni NWs/C-air catalysts with ultrahigh activity and stability toward hydrogen evolution reaction (HER) in alkaline media [68]. They synthesized different composition-segregated Pt-Ni NWs by adjusting the amount of $Ni(acac)_2$, and then loaded on carbon support for further annealing under air or H_2. Annealing in air, the surface of the Pt-Ni NWs produced a rich NiO interface relative to that in H_2. A battery of characterizations distinctly stated that obvious changes occurred with the formation of phase interface with respect to pristine NWs, such as crystal structure and valence state. The as-obtained Pt-Ni NWs/C-air catalysts not only provided a suitable driving force for the dissolution of H_2O to produce intermediate H_{ads} but also possessed a more remarkable electrostatic affinity with OH^- on the interface of NiO_x sites than Pt owing to the partial-occupied d-orbitals of Ni^{x+}, resulting in the unprecedented HER performance. Recently, Huang et al. also annealed PtNi NPs in air to form enriched NiO/PtNi interface on the surface of PtNi-O nanoparticles (Fig. 3) [69]. First, they synthesized the octahedral PtNi/C catalyst in DMF solution, and then annealed at 200 °C for 2 h under air conditions to obtain PtNi-O/C. The detailed characterizations manifested that Ni atoms were segregated and oxidized after annealing in the air, and then the enriched phase interface formed. The PtNi-O/C exhibited a mass activity of 7.23 mA/μg at an overpotential of 70 mV, which was 7.9 times higher than commercial Pt/C for HER.

Considering the gas atmospheres may influence the growth of nanocrystals, Wang's group developed hydrogen assisted solution route (HASR) to prepare trimetallic ultrathin Pt-Mo-Ni NWs [70]. In this case, H_2 acted as a reducing and structure-directing agent. The HAADF-STEM images showed that the obtained NWs have an ample undercoordination atoms around the surface, which enabled much higher power density for ethanol oxidation reaction (EOR) than the state-of-the-art catalysts. CO stripping experiments and DFT simulations demonstrated that introducing Mo atoms in NWs ensured the catalyst with enhanced durability.

Atomic layer coating

It is well known that precious metal catalysts possess excellent catalytic activities, but their high costs greatly hamper their practical applications. Decorating the metal surface with a small amount of foreign metal at the atomic level not only reduces the cost of noble metal catalysts effectively, but also drastically enhances the catalytic performance due to synergistic effects [71]. The catalytic performance of metal@Pt catalyst, for example, can be tuned by altering the thickness of the Pt shell. Simultaneously, the stability

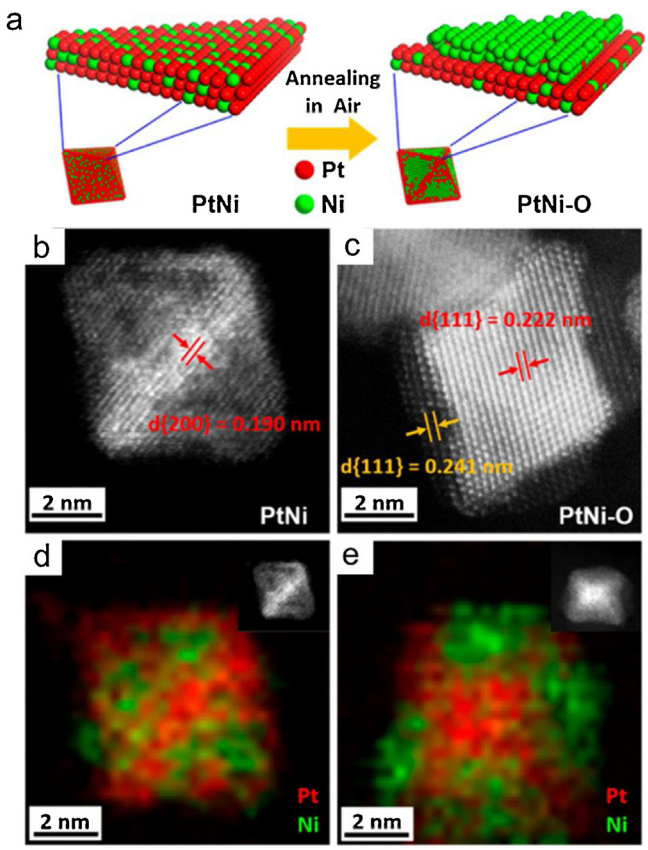

Fig. 3. (a) Schematic illustration of PtNi/C to PtNi-O/C transformation via annealing in the air, HAADF-STEM images of octahedral nanoparticles (b) PtNi/C, (c) PtNi-O/C, EDS maps of octahedral nanoparticles (d) PtNi/C, (e) PtNi-O/C. Inset images in panels d and e are corresponding HAADF-STEM images of mapped nanoparticles.
Reprinted with permission from Ref. [69]. Copyright 2018, American Chemical Society.

of the catalyst increases due to interactions between the Pt shell and the matrix. The atomic layer coating strategy requires precisely tuning the synthetic parameters, such as amount of precursor, injection rate, reaction temperature and so on. For example, Xia and coworkers used an atomic layer by layer deposition strategy to precisely prepare $Pd@Pt_{nL}$ nanostructures (where n is the number of atomic layers) [72]. The thickness of Pt shells could be easily controlled by choosing appropriate amount of the Pt precursor (Fig. 4). It is noteworthy that the introduction of a certain amount of Pt precursor into the growth solution through a syringe pump at a slow rate and high reaction temperature allows for successful coating of ultrathin Pt atoms on the surface of Pd nanocubes. For ORR, the catalytic properties of $Pd@Pt_{nL}$ are closely related with the thickness of Pt shell. The $Pd@Pt_{2\text{-}3L}$ nanocubes exhibited the highest specific activity among all of the $Pd@Pt_{nL}$ catalysts due to the ligand and strain effects, while the $Pd@Pt_{4L}$ and $Pd@Pt_{6L}$ with thicker Pt overlayers showed enhanced stability. The similar strategy can be extended to prepare $Pd@Pt_{nL}$ (n = 2–5) octahedra, by using octahedral Pd as seeds and Pt as shells [73]. Compared to tuning the thickness of the shell, more research efforts are focused on adjusting the shape and composition of the core [74]. For example, Xia et al. deposited a few layers of Pt on Pd nanocubes and Pd octahedron [75], followed by selectively etching away the Pd templates. Thus, the Pt cubic nanocages and nano-octahedral with walls as thin as three atomic layers were obtained, both of which showed high electrocatalytic activity towards the reduction of oxygen. Besides, coating Ir shell on Pd cubes and octahedra to form Pd@Ir cubes and octahedra can also be achieved by using the seed-mediated method [76].

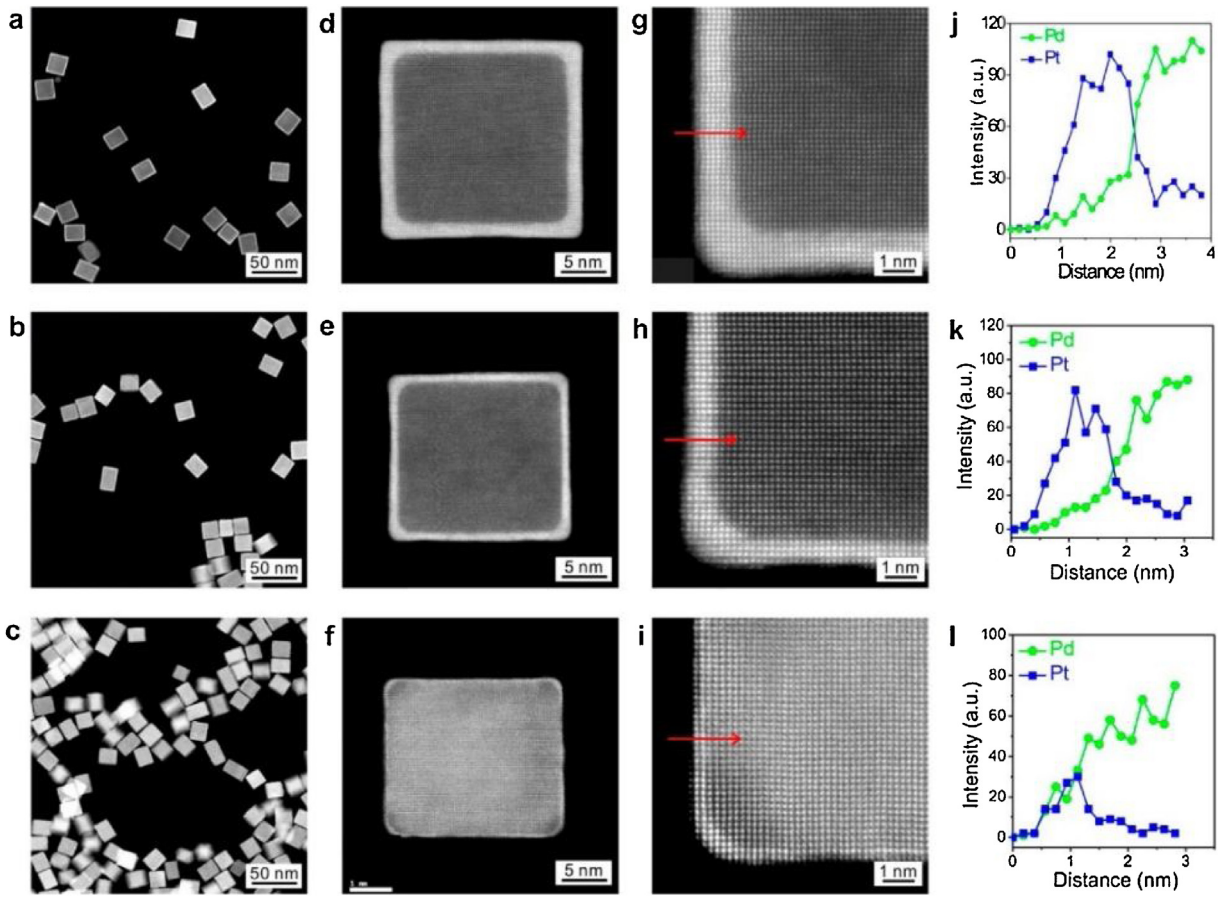

Fig. 4. (a–c) Low-magnification HAADF-STEM images showing a large number of (a) Pd@Pt_{6L}, (b) Pd@Pt_{4L}, and (c) Pd@Pt_{1L} nanocubes, HAADF-STEM images of individual (d) Pd@Pt_{6L}, (e) Pd@Pt_{4L}, and (f) Pd@Pt_{1L} nanocubes, Atomic-resolution HAADF-STEM images taken from the (g) Pd@Pt_{6L}, (h) Pd@Pt_{4L}, and (i) Pd@Pt_{1L} nanocubes, EDX line scan analyses of the (j) Pd@Pt_{6L}, (k) Pd@Pt_{4L}, and (l) Pd@Pt_{1L} nanocubes along the red arrows marked in (g–i).
Reprinted with permission from Ref. [72]. Copyright 2014, American Chemical Society.

The Pd@Ir nanostructures exhibited the obvious facet dependent catalytic properties for the decomposition of hydrazine, in which Pd@Ir cubes covered by Ir{100} facets showed high H_2 selectivity for the decomposition of hydrazine, as compared to the Pd@Ir octahedra covered by Ir{111} facets (31.8% versus 8.9%). Recently, another interesting method to prepare core-shell nanostructures was reported by Wang's group [77]. Pt_3Ga intermetallic nanocrystals were prepared by one-pot strategy in 1-octadecene/oleylamine mixed solvent. Generally, surfactant can act as a physical barrier limits the reactants to the active sites, severely hampering the activity of the catalyst [60]. In this regard, the surfactant is often removed before catalytic measurement. Amine-protected nanocrystals are usually treated by acetic acid washing under mild reaction condition. After removing the surfactant by using acetic acid-washing, they surprisingly found that Pt_3Ga could be converted to Pt/Pt_3Ga catalyst, which contained two to three atomic-layers of Pt on intermetallic Pt_3Ga. It is noted that acetic acid can not only remove the surfactant to make the surface clean, but also lead Pt_3Ga catalyst to Pt/Pt_3Ga core-shell nanostructures. The atomic layer of Pt possessed 3.2% tensile strain along the [001] direction, as confirmed by atomic resolution HAADF-STEM image. Impressively, the Pt/Pt_3Ga structure with 3.2% tensile strain showed better catalytic performance than those of its unstrained counterpart and other commercial Pt/C catalysts. This two-step method could make full use of the diverse morphology of metal. It greatly simplified the complexity involved in the multimetallic reaction system, and provided an effective route to the overall design and synthesis of nanocrystals.

Two-dimensional materials have received a lot of attention, due to their fascinating physical and chemical properties. Deposition of single- or few-layers of atoms on the surface of a two-dimensional nanocrystal remarkably influences the inherent properties of the entire structure. However, due to the intrinsic isotropic growth behavior of metals, controllable synthesis of this attractive catalyst is still a challenging task. Hong and coworkers prepared a novel bimetallic Pd/Ru nanoribbons with dimensions of 93.8 ± 17.8 nm (length), 10.2 ± 2.3 nm (width), and 2.7 nm (thickness) in *N, N*-dimethylacetamide and water solution under CO atmosphere (Fig. 5a–c) [78]. HAADF-STEM images showed that the prepared Pd/Ru nanoribbons were composed of atomically dispersed Ru (up to 5.9%) on ultrathin Pd nanoribbons. In this process, ultrathin Pd nanosheets (NSs) with non-flat surfaces were first synthesized by using CO. After introducing $RuCl_3$ into the above solution, Pd/Ru nanoribbons were quickly formed. Results of the quantitative analysis showed that the surface of the Pd was not atomically flat, which indicated that the Ru adatoms located at the steps or edges of the ultrathin Pd nanoribbons. More importantly, the ultrathin Pd/Ru nanoribbons decrease the binding energies of hydrogen and reaction intermediate, thus increasing the catalytic selectivity as compared with the commercial Pd/C and Ru/C catalysts. A similar manipulation was carried out by Zhang's group to prepare ultrathin Pd NSs decorated with submonolayer Ru, namely Pd@Ru NSs, by a seed-mediated growth method (Fig. 5d–f) [79]. In contrast to other reported structures, the ultrathin Pd NSs were incompletely covered by atomically dispersed Ru atoms. The mechanism indicated that the pre-synthesized Pd NSs not only decreased the energy bar-

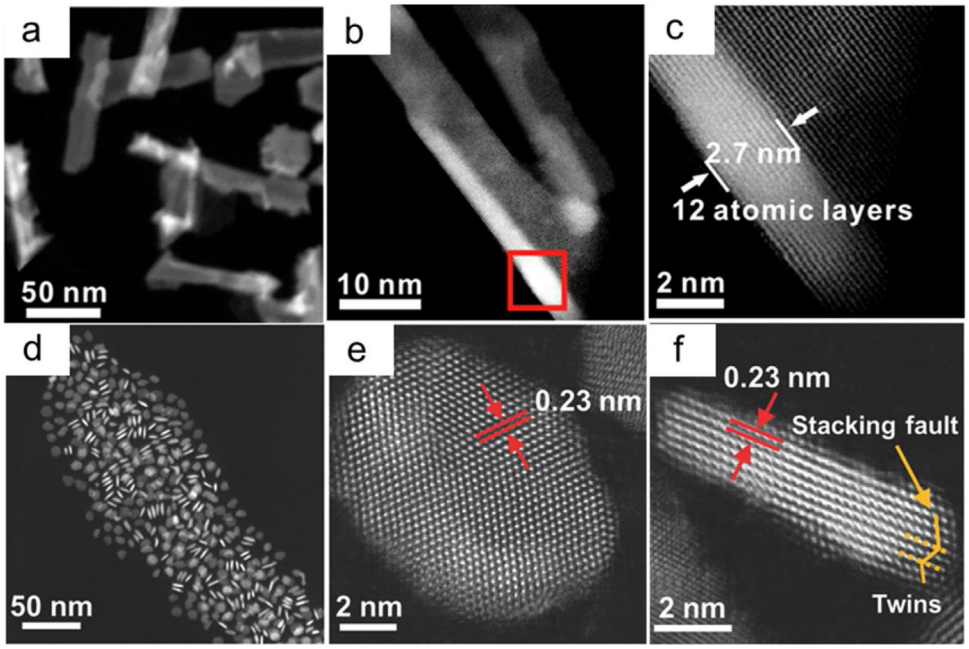

Fig. 5. (a) HAADF-STEM images of the Pd/Ru nanoribbons; Aberration-corrected HAADF-STEM images of (b) a side view of the Pd/Ru nanoribbons; (c) the folded area marked by red squares in (b), showing a thickness of 2.7 nm. Reprinted with permission from Ref. [78]. Copyright 2016, American Chemical Society. (d) HAADF-STEM, and (e, f) aberration-corrected HAADF-STEM images of Pd@Ru NSs. Reprinted with permission from Ref. [79]. Copyright 2016, Wiley-VCH.

rier for nucleation of Ru atoms but also provided nucleation sites for the deposition of Ru atoms on Pd NSs. By taking advantage of the high-density of unsaturated atoms and crystal defect in the nanostructures, the Pd@Ru NSs showed the excellent catalytic properties toward the reduction of 4-nitrophenol and semi-hydrogenation of 1-octyne. How to further optimize the structure or composition of two-dimensional NSs to improve catalytic performance has become a major concern of scientists. Huang and coworkers developed a one-pot strategy to prepare PtPb/Pt core/shell hexagonal nanoplates in non-aqueous medium [80]. In this synthesis, the concentration of Pt and Pb precursors, along with the solvents and surfactants, and reducing agent (ascorbic acid) were all responsible for the formation of well-defined PtPb/Pt nanoplates. Aberration-corrected HAADF-STEM images proved that the obtained PtPb/Pt nanoplates had an intermetallic core comprising of PtPb phase and four uniform atomic layers of Pt shells. Owing to its large tensile strain, this novel structure showed great improvement in terms of both high catalytic activity and durability toward ORR, as compared to PtPb nanoparticles and Pt catalysts.

Although few strategies have been designed for the synthesis of several atomic layers of noble metal on substrate, synthesis of nanostructure that consists of a monolayer of metal atoms on another metal surface, by solution-phase method, has rarely been reported. Recently, for the first time, Hong and coworkers investigated an effective one-step underpotential deposition process to synthesize PdRu nanocrystals [81], in which a monolayer of Ru atoms covered the porous Pd octahedra (Fig. 6). In a typical synthesis, K_2PdCl_4 and $RuCl_3{\cdot}xH_2O$ were dissolved in formaldehyde aqueous solution and heated in an autoclave and at 130 °C for 2 h. The relatively low temperature and shorter reaction time could facilitate the formation of this unique structure. Moreover, the introduction of Ru ions in the typical synthesis could lead to the porous Pd nanoparticles, while solid nanoparticles were obtained without the presence of Ru ions. For semihydrogenation of alkynes, the porous Pd nanoparticles covered with a monolayer of Ru atoms exhibited excellent catalytic activity and stereoselectivity as compared to the Pd catalyst, due to the synergistic effects between the monolayer Ru atoms and porous Pd nanoparticles.

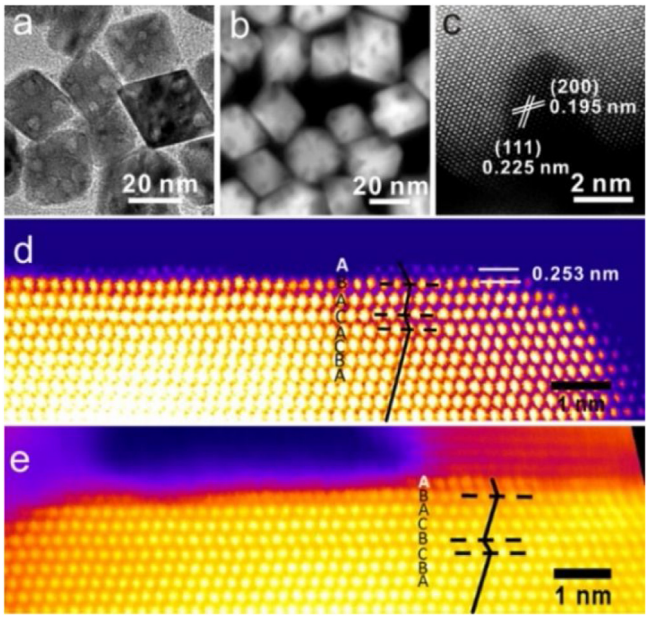

Fig. 6. (a) TEM and (b) HAADF-STEM images of ordered porous octahedral, Atomic resolution aberration-corrected HAADF-STEM images of (c) the porous area of the ordered porous octahedral and (d, e) the surface of octahedra. False color was applied to enhance the contrast.

Reprinted with permission from Ref. [81]. Copyright 2015, American Chemical Society.

Metal doping or substitution

Metal atom doping or substitution means that one metal atom is dispersed in a monodisperse form in another metal material. This protocol allows preparation of nanocrystals with advantages such as low amount of metal used (especially for precious metals) and good model catalyst for recognition of catalytic active center. Generally, there are several main methods for the synthesis of doped

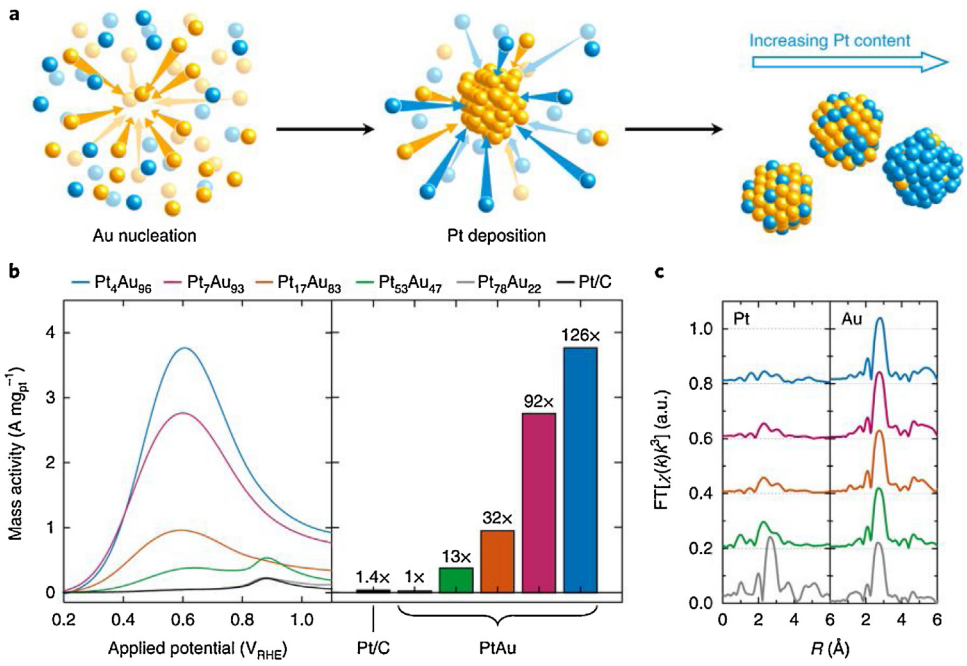

Fig. 7. (a) Illustration of the nanoparticle formation via the reduction of solvated ions, (b) Pt mass-normalized anodic sweeps obtained from PtAu nanoparticle catalysts in an electrolyte that contained 0.1 M concentrations of both $HClO_4$ and HCOOH, with the peak currents graphed for comparison (left), (c) The plotted FT-EXAFS spectra obtained from Pt and Au L_3-edge absorption spectra of PtAu nanoparticles illustrate the drastic undercoordination of Pt atoms in low-Pt content samples.
Reprinted with permission from Ref. [82]. Copyright 2018, Nature Publishing Group.

or isolated dispersed nanostructures between metals, which might achieve the doping in different dimensions.

One straightforward strategy is to synthesize from the mixture of precursors in the liquid phase by a facile wet chemical method. Zhang et al. synthesized a series of catalysts with Pt single atom distributed on the surface of Au nanoparticle via a facile analogous colloidal method (Fig. 7) [82]. In terms of PtAu nanoparticles with tailored surface, the catalysts could be classified as Au with single-atom Pt sites (Pt_7Au_{93} and Pt_4Au_{96}), Au with Pt cluster sites ($Pt_{17}Au_{83}$), and core-shell ($Pt_{78}Au_{22}$ and $Pt_{53}Au_{47}$). Among the classifications, Pt_4Au_{96}, with an enhanced forward current density of 3.77 A mg_{Pt}^{-1} for formic acid electrooxidation was manifested as compared with the core-shell $Pt_{78}Au_{22}$ and commercial Pt/C. DFT simulations and the atomic resolution HAADF-STEM images proved that the Pt_4Au_{96} with single-atom Pt surface sites tightly surrounded by Au atoms ensured its excellent catalytic activity. Furthermore, Zeng's group achieved Pt single atom on Ni NCs via the galvanic replacement between Ni NCs and Pt precursor (Fig. 8) [83]. The pre-prepared Ni NCs were dispersed in hexane, maintained at 50 °C for 10 min, and then Pt species were added by syringe pump under magnetic stirring. Different concentrations of Pt single atom could be embedded in the surface of Ni NCs by varying the amount of added Pt precursor. The Pt_1/Ni NCs manifested much higher activity and selectivity toward selective hydrogenation of 3-nitrostyrene than Pt single atoms loaded on other substrates (such as, active carbon, TiO_2, SiO_2, and ZSM-5). The Pt_1/Ni NCs owned low energy barriers for H dissociation and diffusion so that realized spontaneous dissociation of H_2 on Pt sites as well as H atoms readily diffusion on Ni NCs.

Moreover, some groups used single atom alloys (SAAs) catalysts to depict this unique composition (low content components in the alloy catalysts isolated from each other). For example, Sykes's group fabricated Pd-Cu single atom alloys (SAAs) catalysts for selective hydrogenation of styrene and acetylene [84]. They demonstrated that isolated Pd atoms on partial Cu surface fundamentally decrease the energy barrier to both the adsorption and desorption process of H species by high-resolution scanning tunneling microscopy. The feature of unforced H dissociation at Pd sites and weak binding to Cu finally contributed to the higher catalytic activity than pure Cu or Pd metal. Sykes's group also prepared Pt-Cu SAAs catalysts by injecting desired amounts of H_2PtCl_6 into a suspension of Cu/γ-Al_2O_3 [85]. Aberration-corrected HAADF-STEM characterization showed that there was less than 1 Pt atom in every 100 Cu atoms. Although isolated Pt atom geometries enabled the activation and spillover of H, the inferior capability to cleavage the C—C bond resulted in loss of selectivity and catalyst deactivation. The Pt-Cu SAAs supported on γ-Al_2O_3 well solved this contradiction, and showed high activity and selectivity for butadiene hydrogenation under mild conditions. In addition to isolate noble atoms (e.g. Pt, Pd) on transition metal surface, isolating transition metal in noble metal lattice is also an effective strategy for enhancing the catalytic performance. Xiong et al. synthesized different components of Pd_xCu_1-TiO_2 hybrid structures in aqueous solution containing TiO_2 NSs [86]. They prepared a series of Pd_xCu_1 alloys by adjusting the concentration of Pd and Cu precursors. Among them, the Pd_7Cu_1-TiO_2 photocatalyst with isolated Cu atoms into the Pd lattice showed high selectivity for conversion of CO_2 to CH_4. A series of characterizations demonstrated that the isolating Cu atoms in Pd lattice not only provides a paired Cu-Pd sites for CO_2 adsorption, but also elevates the d-band centers of Cu sites for CO_2 activation.

Doping foreign metals on ultrafine nanomaterials (e.g. ultrathin NWs, NSs) can further magnify the advantages of ultrathin structure, consequently leading to the promising catalytic performance. Zeng et al. prepared Rh-doped Pt NWs (Fig. 9) by co-reduction of $Rh(acac)_2$ and $Pt(acac)_2$ in didecyldimethylammonium bromide (DDAB) and OAm mixed solutions with the introduction of $W(CO)_6$ [87]. In this synthetic system, DDAB acted as a soft template, $W(CO)_6$ increased the reduction kinetics for the formation of such NWs. For ORR performance, the Rh-doped Pt NWs/C catalyst showed enhanced mass activity and durability as compared with Pt NWs/C and Pt/C catalysts. The EXAFS and DFT calculations indicated that doping Rh into the Pt NWs not only changed the compressive strain and ligand effect of the NWs, but also heightened the vacancy formation energy of the Pt atoms, leading to the enhanced

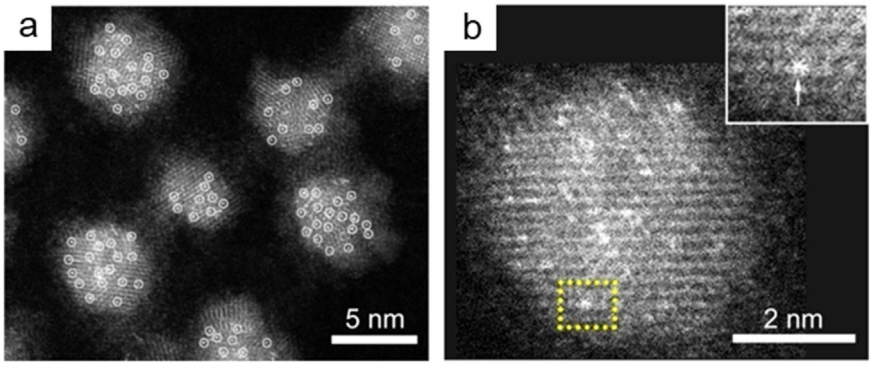

Fig. 8. (a) HAADF-STEM image of 1.0% Pt_1/Ni nanocrystals, Pt single atoms marked in white circles were uniformly embedded in the surface of Ni nanocrystals, (b) HAADF-STEM image of an individual 1.0% Pt_1/Ni nanocrystal. The inset image derives from the yellow box in panel b. A Pt single atom was marked by the white arrow.
Reprinted with permission from Ref. [83]. Copyright 2018, American Chemical Society.

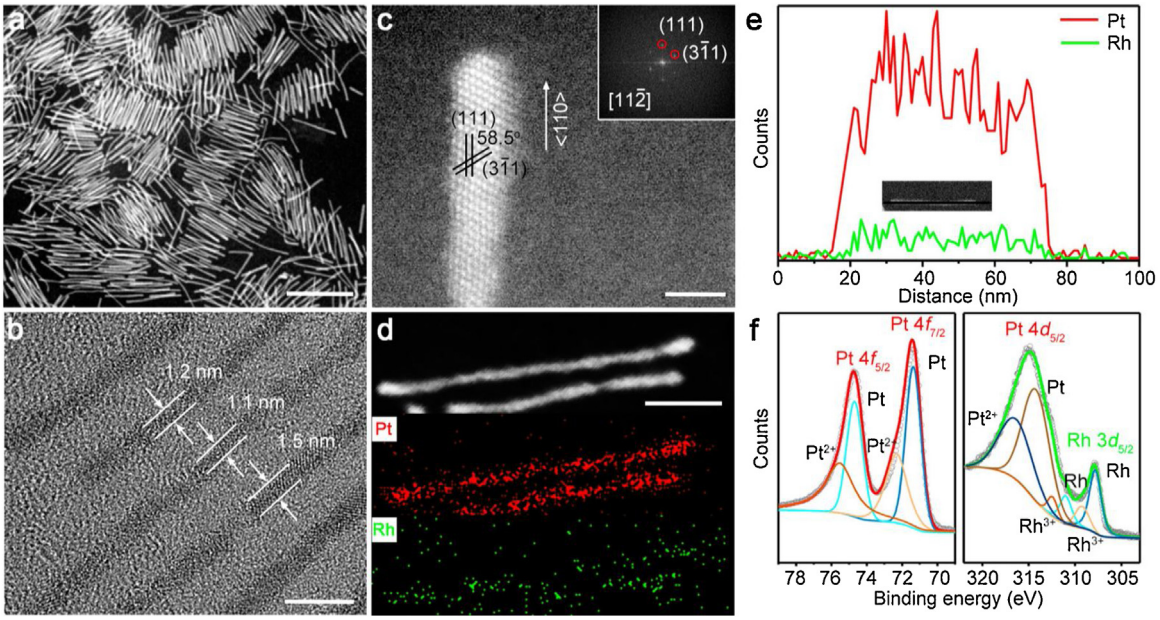

Fig. 9. (a) HAADF-STEM image of Rh-doped Pt NWs, Scale bar, 50 nm, (b) TEM image. Scale bar, 5 nm, (c) Atomic-resolution HAADF-STEM image, the inset shows the corresponding FFT pattern. Scale bar, 2 nm, (d) EDX mapping of Pt and Rh. Scale bar, 10 nm, (e) EDX line-scanning profile, (f) Pt and Rh XPS spectra recorded from Rh-doped Pt NWs.
Reprinted with permission from Ref. [87]. Copyright 2017, American Chemical Society.

ORR performance. For ultrathin NSs, very recently, Wang's group synthesized Co-substituted Ru NSs, in which atomically dispersed Co were isolated in Ru lattice [88]. The Co-substituted Ru NSs were synthesized by co-reduction of Ru and Co precursors in the mixed solutions containing OAm and heptanol. Via increasing the content of Co precursor in the above synthetic system, Ru-Co alloy was formed. DFT studies reveals that single Co atom substituted nanostructures could significantly reduce the energy barrier of water dissociation as demonstrated by DFT calculation, leading to the much higher performance toward HER than Ru-Co alloy and other reported Pt-free catalysts.

What's more, the catalytic activity can be further improved by tuning the coordination environment of single atoms with multiple atoms. For the first time, Hong et al. achieved the fabrication of Cu-Pt dual sites alloyed with Pd nanorings (NRs) by two-step approach [89]. In the first step, the composite of atomically dispersed Cu on ultrafine Pd NRs was generated by adding Cu substances into Pd NSs under the CO atmosphere. Then the as-obtained Pd/Cu NRs were put into hydrochloric acid (HCl) solution containing tiny amounts of Pt precursor and the desirable catalyst was obtained under ultrasonic bath for 45 min. The EXAFS analysis showed strong Cu-Pt coordination peaks without the characteristic peaks of Cu-Cu and Pt-Pt, suggesting that Cu-Pt dual sites were dispersed on the Pd NRs at the atomic level. Electrochemical tests demonstrated that atomically dispersed Cu-Pt dual sites alloyed with Pd NRs possessed outstanding HER catalytic activity as compared with Pt/C.

Intermetallic compounds

Intermetallic compounds with fixed stoichiometries and highly ordered atomic structures have attracted tremendous attention in the fields of material chemistry and catalysis. Compared to disordered alloys, the ordered alloy nanostructures can provide strong interactions and orbit rehybridization of atoms to achieve high catalytic performance. However, due to the high order of its structure, the synthesis of intermetallic compounds often requires higher energy, making its synthesis more difficult as compared to alloy compounds. Exploration of new synthetic reactions to prepare intermetallic compounds with specific structures is a challenging task in nanoscience. Previously, Li and co-workers developed

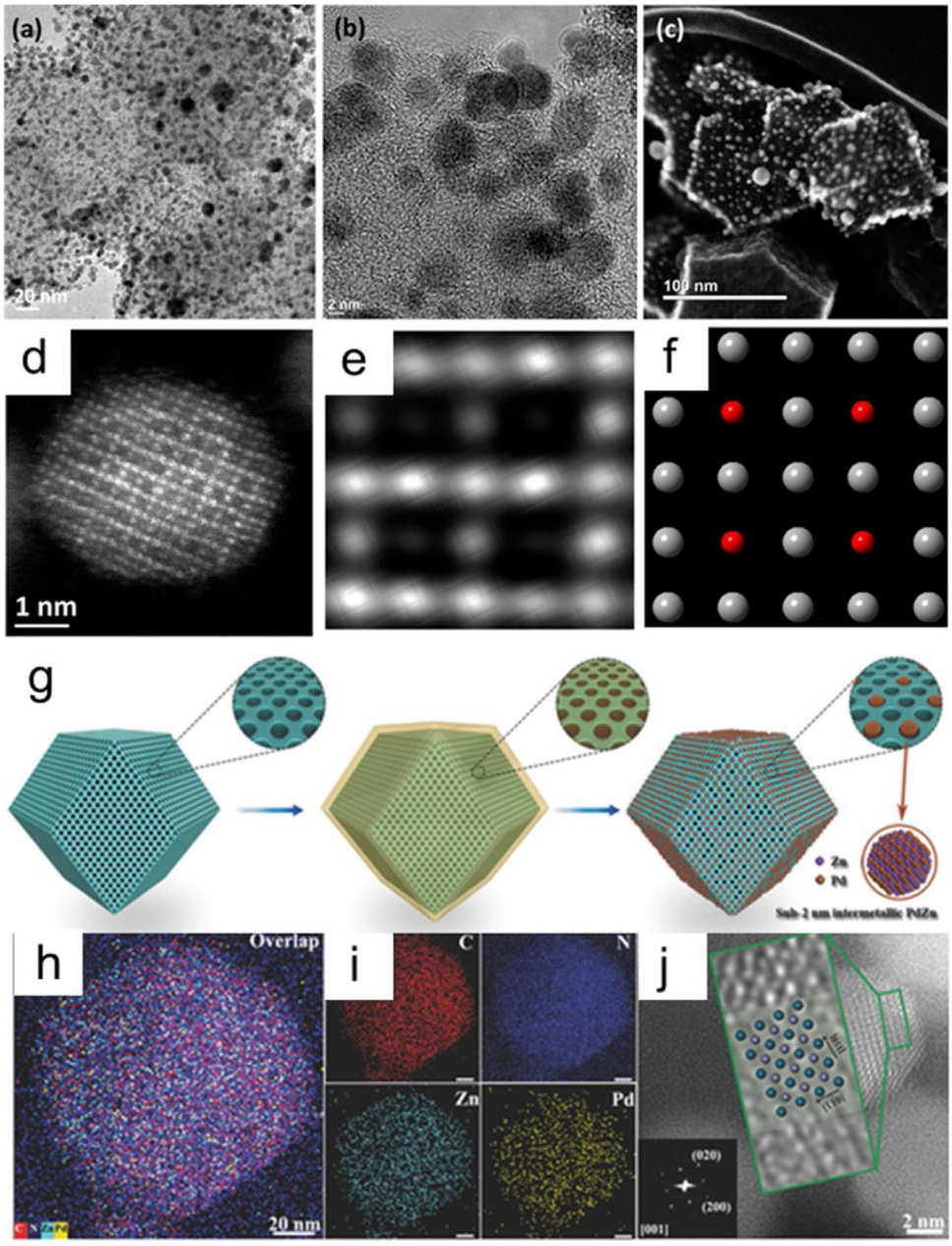

Fig. 10. (a) TEM, (b) HRTEM, (c) Dark field STEM images of Pt/40Co-NC-900 catalyst, (d) Atomic resolution HAADF-STEM image of Pt_3Co nanoparticle, (e) A crop of the superlattice feature from (d), (f) The simulated HAADF-STEM images of L12 ordered Pt_3Co close along [100]. Reprinted with permission from Ref. [98]. Copyright 2018, American Chemical Society. (g) Schematic preparation process of the PdZn-sub-2@ZIF-8C using a MOF-confined co-reduction strategy, (h, i) EDS elementary mapping images of the PdZn-1.2@ZIF-8C, Scale bar, 20 nm, (j) High-resolution HAADF-STEM image of PdZn-10/ZIF-8C. Reprinted with permission from Ref. [99]. Copyright 2018, Wiley-VCH.

a facile and general method for synthesis of bimetallic nanocrystals using octadecylamine (ODA) solely as a solvent, surfactant, as well as a reducing agent [90–94]. By employing this typical system, dozens of bimetallic alloys and intermetallic nanocrystals have been successfully synthesized. However, a systematic regulation of morphologies of intermetallic compounds is still a challenging task. Recently, three intermetallic Pt_3Sn NCs with different surface structures (cubic, concave cubic, and defect-rich) were prepared in *N*, *N*-dimethylformamide medium, on the basis of large electronegativity differences between Pt and Sn [95]. By careful investigation of the growth process, a "large electronegativity difference-induced/etching-assisted/diffusion-terminated" growth mechanism was proposed for the preparation of intermetallic compounds. Interestingly, Pt_3Sn NCs with different surface structures show obvious surface-dependent catalytic properties for formic acid oxidation. Intermetallic nanostructures and defect-rich surfaces endow the nanocrystals with excellent catalytic activity and stability. Apart from regulating the electronegativities of metals, the surface structure of intermetallic compounds can also be regulated by using small molecules or functional groups. Huang and coworkers reported a wet-chemical approach to prepare Pd_3Pb intermetallic nanomaterials with three different concave degrees [96], namely, nanocubes, slightly concave nanocubes, and concave nanocubes. A series of contrast experiments revealed that halogen ions were responsible for the formation of nanocubes. Meanwhile, the formation of Pd_3Pb slightly concave nanocubes and concave nanocubes could be attributed to the effects of −CHO and −COOH groups, respectively. Amongst intermetallic compounds, Cu-based intermetallic nanostructures, such as Au-Cu, Pd-Cu, and Pt-Cu have attracted more attention due to their wide applications in elec-

Table 1
Summary of structure regulation of noble-metal-based nanomaterials.

Strategies	Morphologies	Catalytic properties
Surface engineering	Starlike corroded $PtNi_3$	MOR/ Hydrogenation of nitrobenzene
	Pt_3Ni nanoframes	ORR
	Au island on Pt_3Ni nanoframes	MOR/Hydrogenation of 4-nitrobenzaldehyde
	PtNi nanowires to jagged Pt nanowires	ORR
	PtCo zigzag nanowires	Electrochemical detection of small molecules/ORR
	Pt-Ni nanowires/C-air	HER
	PtNi-O/C nanoparticles	HER
	Pt-Mo-Ni nanowires	EOR
	$Pd@Pt_{nL}$ nanocubes	ORR
	$Pd@Pt_{nL}$ octahedra	ORR
	$Pd@Pt_{nL}$ cubic nanocages, $Pd@Pt_{nL}$ octahedral nanocages	ORR
Atomic layer coating	Pd@Ir cubes and octahedra	Decomposition of hydrazine
	Pt/Pt_3Ga	EOR
	Pd/Ru nanoribbons	Hydrogenation of allyl benzyl ether
	Pd@Ru nanosheets	Reduction of 4-nitrophenol, Semi-hydrogenation of 1-octyne
	PdPb/Pt hexagonal nanoplates	ORR
	Ru atoms covered Pd nanoparticles	Semi-hydrogenation of alkynes
Metal doping/substitution	Pt_4Au_{96} nanoparticles	Formic acid electrooxidation
	Pt_1/Ni nanocrystals	Hydrogenation of 3-nitrostyrene
	Pd-Cu single atom alloys	Hydrogenation of styrene and acetylene
	Pt-Cu single atom alloys	Butadiene hydrogenation
	Pd_xCu_1/TiO_2 hybrid structures	Photocatalytic conversion of CO_2
	Rh-doped Pt nanowires	ORR
	Co-substituted Ru nanosheets	HER
	Pd/Cu-Pt nanorings	HER
Intermetallic compounds	Pt_3Sn nanocubes	FOR
	Pd_3Pb nanocubes	Semi-hydrogenation of phenylacetylene
	AuCu nanoparticles	CO_2 reduction
	Pt_3Co nanoparticle	ORR
	PdZn, PtZn nanoparticles	Hydrogenation of acetylene

Note: MOR stands for methanol oxidation reaction, EOR stands for ethanol oxidation reaction, FOR stands for formic acid oxidation reaction.

trocatalytic reactions. For example, Li designed a seed-mediated method for the preparation of Cu_3Au and CuAu intermetallic compounds [97], in which Au formed the core and Cu diffused into the lattice of Au. Pd-Cu and Pt-Cu alloys can be obtained similarly by simply replacing Au crystals with Pd or Pt, respectively. Furthermore, Yang and coworkers found that higher temperatures and longer reaction times are essentially required for the formation of ordered Au-Cu lattices [53]. Such ordered nanostructures find applications widely in energy-related catalytic reactions and exhibit excellent catalytic performance.

So far, solution-phase methods have been generally used for the synthesis of intermetallic compounds. Before the evaluation of performance, the obtained intermetallic compound has to be loaded on a carbon support. However, due to weak interactions of the catalyst with the carbon support, the catalyst readily forms aggregates or gets dissolved during the reaction process, resulting in reduced catalytic durability. In addition, the surfactant attached on the surface of intermetallic compound also affects the catalytic performance. Thus, developing a new method to resolve the above issues is expected to further improve its activity and stability.

Recently, MOF-confined strategy was employed for the synthesis of intermetallic compounds. For example, Wu and coworkers designed an ingenious strategy to synthesize ordered Pt_3Co intermetallic compound [98], which was embedded into zeolitic imidazolate framework (ZIF) -derived carbon nanostructures (Fig. 10a-f). In the first step of the synthesis, Co-doped ZIF nanocrystals were prepared as the precursors for Co-doped carbon. Then Pt nanoparticles were supported onto Co-doped carbon, which was then followed by a facile thermal treatment step. The atomically dispersed Co atoms diffused into Pt nanoparticles during the high temperature treatment, which ultimately resulted in the formation of highly ordered Pt_3Co intermetallic structures. In the synthesis of these Pt_3Co intermetallic compounds, the doping amount of Co and subsequent heating temperatures for Co diffusion were found to be crucial. Taking advantage of their unique geometries and electronic structures, the ordered Pt_3Co particles possessed not only high onset potential (1.05 versus 1.02 V), and half-wave potentials (0.92 versus 0.86 V), in comparison to Pt/C, but also superior stability (losing only 12 mV on half-wave potential after 30,000 potential cycles between 0.6 and 1.0 V). Based on the MOF materials, other intermetallic compounds with different compositions can also be prepared. Chen and co-workers reported another similar method to prepare intermetallic PdZn nanoparticles within ZIF-8 derived carbon using a MOF-confined co-reduction strategy (Fig. 10g–i) [99]. Results of characterization demonstrated that these sub-2 nm PdZn nanoparticles with atomically-ordered structure were effectively embedded into the regular pores of the ZIF-8-C. The ultra-small intermetallic PdZn nanoparticles showed higher selectivity towards the hydrogenation of acetylene than the larger-sized intermetallic PdZn. Theoretical studies reveal that ultra-small intermetallic PdZn nanoparticles are more favorable for acetylene hydrogenation and ethylene desorption. More importantly, this strategy is also applicable for the synthesis of intermetallic PtZn nanoparticles, and is expected to be employed for the synthesis of other intermetallic nanoparticles with ultra-small sizes by rational functionalization of MOFs. This work not only enriches our knowledge of the synthetic methodology of intermetallic compounds, but also provides a rich source of information regarding the composition, size, and structure of the intermetallic compounds for applications in industrial catalysis.

Conclusions and prospects

Due to the growing demand for global energy and fast depletion of non-renewable energy resources, development of high-efficiency catalysts has become a major requirement for sustainable development and the national economy. The traditional “controllable synthesis” methods still fail to address some structure-activity relationships well, and there are contradictions in elaborating some principles. Precise synthesis of catalysts came

into existence, and quickly became a hot topic in the field of materials and chemistry, attracting wide attention. Several atomic-level controllable synthetic methods have been employed for synthesis of nanocrystals with precision. Through these methods, a series of surface structure-determined nanocrystals were synthesized (Table 1), which included the highly opened three-dimensional Pt_3Ni nanoframes, monolayer Ru atoms covered porous Pd octahedral, monoatomic Co substituted Ru nanosheets, intermetallic Pt_3Sn NCs, etc. These well-defined structures exhibited excellent catalytic performance towards oxygen reduction reaction, semihydrogenation of alkynes, hydrogen evolution reaction, formic acid oxidation reaction, etc.

Although some methods of controlled synthesis have been developed, it is still complicated to synthesize nanocrystals with precision, since the mechanism of nucleation in the synthesis of nanocrystals is unclear. In-situ XAFS technique provides the most realistic data for structural changes in the nucleation process of nanocrystals. It helps to objectively and quantitatively evaluate the nanocrystal nucleation and growth processes. Once the nucleation mechanism is well understood, the rational design of catalysts becomes possible. Another important aspect of nanosynthesis at the atomic scale is the effect of ligands. The type and dosage of ligands greatly influence the electronic structure and catalytic properties of nanocrystals. It is very important to understand the coordination interactions between the ligand and the metal nanoparticles through theoretical calculations and qualitative characterizations. For the catalytic reaction process, it is often assumed that the obtained catalyst structure is correlated to its catalytic performance. In fact, it should be noted that the initial structure of the catalyst may not be the real structure of the catalyst in the reaction. Uniformities in the size and morphology of the nanocrystal at an atomic level provide an essential basis for observation and study of structural changes, before and after the reaction. A detailed characterization of the catalyst after reaction is necessary. Furthermore, relation between the fine structure (coordination number, bond length, coordination atom, oxidation state, bond polarity, etc.) of the catalyst and its performance, need to be studied. The observation of the structure and performance testing at the surface/interface of nanosystems still needs further improvements and innovation. Some model catalytic systems can be designed to understand the correlation between catalyst structure and performance at the atomic level, which may enable to set guidelines for developing catalysts with excellent performance. At present, the strategy for nanocrystal synthesis at the atomic level is just limited to the laboratory-level of research. More attention should be paid to large-scale production of catalysts with controllable structure. Our final goal is to achieve precise synthesis of nanocrystal structure at the atomic level, while also achieving mass production of the catalysts.

Acknowledgments

This work was supported by the National Key R&D Program of China (2016YFA0202801), the National Natural Science Foundation of China (21671117, 21871159, 21890383).

References

[1] L. Zhang, Z.J. Zhao, J.L. Gong, Angew. Chem. Int. Ed. 56 (2017) 2–30.
[2] H. Mistry, A.S. Varela, S. Kühl, P. Strasser, B.R. Cuenya, Nat. Rev. Mater. 1 (2016) 16009–16023.
[3] H.L. Liu, F. Nosheen, X. Wang, Chem. Soc. Rev. 44 (2015) 3056–3078.
[4] V.R. Stamenkovic, B. Fowler, B.S. Mun, G. Wang, P.N. Ross, C.A. Lucas, N.M. Markovic; Science 315 (2007) 493–497.
[5] S.B. Liu, H.B. Tao, L. Zeng, Q. Liu, Z.H. Xu, Q.X. Liu, J.L. Luo, J. Am. Chem. Soc. 139 (2017) 2160–2163.
[6] W. Yu, M.D. Porosoff, J.G. Chen, Chem. Rev. 112 (2012) 5780–5817.
[7] T.T. Sun, L.B. Xu, D.S. Wang, Y.D. Li, Nano Res. (2019), http://dx.doi.org/10.1039/C9NH00036D.
[8] M.K. Debe, Nature 486 (2012) 43–51.
[9] M.V. Kovalenko, L. Manna, A. Cabot, Z. Hens, D.V. Talapin, C.R. Kagan, X.I. Klimov, A.L. Rogach, P. Reiss, D.J. Milliron, P.G. Sionnnest, G. Konstantatos, W.J. Parak, T. Hyeon, B.A. Korgel, C.B. Murray, W. Heiss, ACS Nano 9 (2015) 1012–1057.
[10] Y. Jiang, S.D. Huo, T. Mizuhara, R. Das, Y.W. Lee, S. Hou, D.F. Moyano, B. Duncan, X.J. Liang, V.M. Rotello, ACS Nano 9 (2015) 9986–9993.
[11] M.C. Daniel, D. Astruc, Chem. Rev. 104 (2004) 293–346.
[12] Z. Ma, S. Dai, ACS Catal. 1 (2011) 805–818.
[13] Y. Tan, X.Y. Liu, L. Li, L.L. Kang, A.Q. Wang, T. Zhang, J. Catal. 364 (2018) 174–182.
[14] Y. Jiang, H. Zhao, Y.Q. Lin, N.N. Zhu, Y.R. Ma, L.Q. Mao, Angew. Chem. Int. Ed. 49 (2010) 4800–4804.
[15] H.S. Gandhi, G.W. Graham, R.W. McCabe, J. Catal. 216 (2003) 433–442.
[16] L.C. Liu, A. Corma, Chem. Rev. 118 (2018) 4981–5079.
[17] F.F. Tao, L. Nguyen, S.A. Zhang, Y.Y. Li, Y. Tang, L. Zhang, A.I. Frenkel, Y.N. Xia, M. Salmeron, Nano Lett. 16 (2016) 5001–5009.
[18] Y.Z. Lu, L. Thia, A. Fisher, C.Y. Jung, S.C. Yi, X. Wang, Sci. China Mater. 60 (2017) 1109–1120.
[19] M.X. Yang, W.X. Wang, K.D. Gilroy, Y.N. Xia, Nano Lett. 17 (2017) 5682–5687.
[20] Y. Yang, J.Y. Liu, Z.W. Fu, D. Qin, J. Am. Chem. Soc. 136 (2014) 8153–8156.
[21] X.L. Sun, D.G. Li, Y. Ding, W.L. Zhu, S.J. Guo, Z.L. Wang, S.H. Sun, J. Am. Chem. Soc. 136 (2014) 5745–5749.
[22] S. Yang, H. Lee, ACS Catal. 3 (2013) 437–443.
[23] L.L. Zou, J. Fan, Y. Zhou, C.M. Wang, J. Li, Z.Q. Zou, H. Yang, Nano Res. 8 (2015) 2777–2788.
[24] X.T. Chen, C.H. Si, Y. Wang, Y. Ding, Z.H. Zhang, Nano Res. 9 (2016) 1831–1843.
[25] T. Zhang, S.A. Liao, L.X. Dai, J.W. Yu, W. Zhu, Y.W. Zhang, Sci. China Mater. 61 (2018) 926–938.
[26] W. Ye, Z.T. Sun, C.M. Wang, M.S. Ye, C.H. Ren, R. Long, X.S. Zheng, J.F. Zhu, X.J. Wu, Y.J. Xiong, Nano Res. 11 (2018) 3313–3326.
[27] Q. Li, S.F. Ji, M.F. Li, X.F. Duan, Sci. China Mater. 61 (2018) 1339–1344.
[28] Y.C. Pi, Q. Shao, X. Zhu, X.Q. Huang, ACS Nano 12 (2018) 7371–7379.
[29] J.B. Ding, L.Z. Bu, S.J. Guo, Z.P. Zhao, E.B. Zhu, Y. Huang, X.Q. Huang, Nano Lett. 16 (2016) 2762–2767.
[30] H.F. Lv, Z. Xi, Z.Z. Chen, S.J. Guo, Y.S. Yu, W.L. Zhu, Q. Li, X. Zhang, M. Pan, G. Lu, S.C. Mu, S.H. Sun, J. Am. Chem. Soc. 137 (2015) 5859–5862.
[31] N.N. Du, C.M. Wang, R. Long, Y.J. Xiong, Nano Res. 10 (2017) 3228–3237.
[32] L.M. Zeng, X.Z. Cui, J.L. Shi, Sci. China Mater. 61 (2018) 1557–1566.
[33] Z.C. Zhang, G.G. Liu, X.Y. Cui, B. Chen, Y.H. Zhu, Y. Gong, F. Saleem, S.B. Xi, Y.H. Du, A. Borgna, Z.C. Lai, Q.H. Zhang, B. Li, Y. Zong, Y. Han, L. Gu, H. Zhang, Adv. Mater. 30 (2018) 1801741–1801748.
[34] N. Becknell, Y. Son, D. Kim, D.G. Li, Y. Yu, Z.Q. Niu, T. Lei, B.T. Sneed, K.L. More, N.M. Markovic, V.R. Stamenkovic, P.D. Yang, J. Am. Chem. Soc. 139 (2017) 11678–11681.
[35] C.Z. Li, Q. Yuan, B. Ni, T. He, S.M. Zhang, Y. Long, L. Gu, X. Wang, Nat. Commun. 9 (2018) 3702–3711.
[36] X.Q. Huang, Z.P. Zhao, L. Cao, Y. Chen, E.B. Zhu, Z.Y. Lin, M.F. Li, A.M. Yan, A. Zettl, Y.M. Wang, X.F. Duan, T. Mueller, Y. Huang, Science 348 (2015) 1230–1234.
[37] S.I. Choi, M.H. Shao, N. Lu, A. Ruditskiy, H.C. Peng, J. Park, S. Guerrero, J.G. Wang, M.J. Kim, Y.N. Xia, ACS Nano 8 (2014) 10363–10371.
[38] Y.N. Qin, M.C. Luo, Y.J. Sun, C.J. Li, B.L. Huang, Y. Yang, Y.J. Li, L. Wang, S.J. Guo, ACS Catal. 8 (2018) 5581–5590.
[39] L.Z. Bu, S.J. Guo, X. Zhang, X. Shen, D. Su, G. Lu, X. Zhu, J.L. Yao, J. Guo, X.Q. Huang, Nat. Commun. 7 (2016) 11850–11860.
[40] H.A. Gasteiger, S.S. Kocha, B. Sompalli, F.T. Wagner, Appl. Catal. B Environ. 56 (2005) 9–35.
[41] Y.J. Wang, N.N. Zhao, B.Z. Fang, H. Li, X.T. Bi, H.J. Wang, Chem. Rev. 115 (2015) 3433–3467.
[42] S.J. Guo, X. Zhang, W.L. Zhu, K. He, D. Su, A.M. Garcia, S.F. Ho, G. Lu, S.H. Sun, J. Am. Chem. Soc. 136 (2014) 15026–15033.
[43] Y. Bing, H. Liu, L. Zhang, D. Ghosh, J. Zhang, Chem. Soc. Rev. 39 (2010) 2184–2202.
[44] Y. Nie, L. Li, Z. Wei, Chem. Soc. Rev. 44 (2015) 2168–2201.
[45] D.S. He, D.P. He, J. Wang, Y. Lin, P.Q. Yin, X. Hong, Y.E. Wu, Y.D. Li, J. Am. Chem. Soc. 138 (2016) 1494–1497.
[46] X. Wang, L.F. Cosme, X. Yang, M. Luo, J.Y. Liu, Z.X. Xie, Y.N. Xia, Nano Lett. 16 (2016) 1467–1471.
[47] Q.C. Feng, S. Zhao, Y. Wang, J.C. Dong, W.X. Chen, D.S. He, D.S. Wang, J. Yang, Y.M. Zhu, H.L. Zhu, L. Gu, Z. Li, Y.X. Liu, R. Yu, J. Li, Y.D. Li, J. Am. Chem. Soc. 139 (2017) 7294–7301.
[48] J.R. Li, Z. Xi, Y.T. Pan, J.S. Spendelow, P.N. Duchesne, D. Su, Q. Li, C. Yu, Z.Y. Yin, B. Shen, Y.S. Kim, P. Zhang, S.H. Sun, J. Am. Chem. Soc. 140 (2018) 2926–2932.
[49] H.Q. Li, R. Yao, D. Wang, J.F. He, M.R. Li, Y.J. Song, J. Phys. Chem. C 119 (2015) 4052–4061.
[50] K.P. Gong, D. Su, R.R. Adzic, J. Am. Chem. Soc. 132 (2010) 14364–14366.
[51] Y.C. Yao, D.S. He, Y. Lin, X.Q. Feng, X. Wang, P.Q. Yin, X. Hong, G. Zhou, Y.E. Wu, Y.D. Li, Angew. Chem. Int. Ed. 55 (2016) 5501–5505.
[52] S.F. Xie, H.C. Peng, N. Lu, J.G. Wang, M.J. Kim, Z.X. Xie, Y.N. Xia, J. Am. Chem. Soc. 135 (2013) 16658–16667.
[53] D. Kim, C.L. Xie, N. Becknell, Y. Yu, M. Karamad, K. Chan, E.J. Crumlin, J.K. Nørskov, P.D. Yang, J. Am. Chem. Soc. 139 (2017) 8329–8336.
[54] T.T. Chao, Y.M. Hu, X. Hong, Y.D. Li, ChemElectroChem 6 (2019) 289–303.

[55] A. Ruditskiy, Y.N. Xia, ACS Nano 11 (2017) 23–27.
[56] D.D. Zhao, Y.C. Pi, Q. Shao, Y.G. Feng, Y. Zhang, X.Q. Huang, ACS Nano 12 (2018) 6245–6251.
[57] S. Zhang, X. Zhang, G.M. Jiang, H.Y. Zhu, S.J. Guo, D. Su, G. Lu, S.H. Sun, J. Am. Chem. Soc. 136 (2014) 7734–7739.
[58] Z.Q. Niu, D.S. Wang, R. Yu, Q. Peng, Y.D. Li, Chem. Sci. 3 (2012) 1925–1929.
[59] J.J. Ge, P. Wei, G. Wu, Y.D. Liu, T.W. Yuan, Z.J. Li, Y.T. Qu, Y. Wu, H. Li, Z.B. Zhuang, X. Hong, Y.D. Li, Angew. Chem. Int. Ed. 57 (2018) 3435–3438.
[60] Z.Q. Niu, Y.D. Li, Chem. Mater. 26 (2014) 72–83.
[61] J.J. Mao, Y.J. Chen, J.J. Pei, D.S. Wang, Y.D. Li, Chem. Commun. 52 (2016) 5985–5988.
[62] J.J. Pei, J.J. Mao, X. Liang, Z.B. Zhuang, C. Chen, Q. Peng, D.S. Wang, Y.D. Li, ACS Sustain. Chem. Eng. 6 (2018) 77–81.
[63] Y.E. Wu, D.S. Wang, Z.Q. Niu, P.C. Chen, G. Zhou, Y.D. Li, Angew. Chem. Int. Ed. 51 (2012) 12524–12528.
[64] C. Chen, Y.J. Kang, Z.Y. Huo, Z.W. Zhu, W.Y. Huang, H.L. Xin, J.D. Snyder, D.G. Li, J.A. Herron, M. Mavrikakis, M.F. Chi, K.L. More, Y.D. Li, N.M. Markovic, G.A. Somorjai, P.D. Yang, V.R. Stamenkovic, Science 343 (2014) 1339–1343.
[65] Y.E. Wu, D.S. Wang, G. Zhou, R. Yu, C. Chen, Y.D. Li, J. Am. Chem. Soc. 136 (2014) 11594–11597.
[66] M.F. Li, Z.P. Zhao, T. Cheng, A. Fortunelli, C.Y. Chen, R. Yu, Q.H. Zhang, L. Gu, B. Merinov, Z.Y. Lin, E.B. Zhu, T. Yu, Q.Y. Jia, J.H. Guo, L. Zhang, W.A. Goddard III, Y. Huang, X.F. Duan, Science 354 (2016) 1414–1419.
[67] M.C. Luo, Y.J. Sun, Y.N. Qin, S.L. Chen, Y.J. Li, C.J. Li, Y. Yang, D. Wu, N.Y. Xu, Y. Xing, L. Wang, P. Gao, S.J. Guo, Chem. Mater. 30 (2018) 6660–6667.
[68] P.T. Wang, K.Z. Jiang, G.M. Wang, J.L. Yao, X.Q. Huang, Angew. Chem. Int. Ed. 55 (2016) 12859–12863.
[69] Z.P. Zhao, H.T. Liu, W.P. Gao, W. Xue, Z.Y. Liu, J. Huang, X.Q. Pan, Y. Huang, J. Am. Chem. Soc. 140 (2018) 9046–9050.
[70] J.J. Mao, W.X. Chen, D.S. He, J.W. Wan, J.J. Pei, J.C. Dong, Y. Wang, P.F. An, Z. Jin, W. Xing, H.L. Tang, Z.B. Zhuang, X. Liang, Y. Huang, G. Zhou, L.Y. Wang, D.S. Wang, Y.D. Li,Sci. Adv. 3 (2017), e1603068.
[71] J.J. Ge, Z.J. Li, X. Hong, Y.D. Li, Chem. Eur. J. 25 (2019) 1–16.
[72] S.F. Xie, S.I. Choi, N. Lu, L.T. Roling, J.A. Herron, L. Zhang, J.H. Park, J.G. Wang, M.J. Kim, Z.X. Xie, M. Mavrikakis, Y.N. Xia, Nano Lett. 14 (2014) 3570–3576.
[73] J.H. Park, L. Zhang, S.I. Choi, L.T. Roling, N. Lu, J.A. Herron, S.F. Xie, J.G. Wang, M.J. Kim, Z.X. Xie, M. Mavrikakis, Y.N. Xia, ACS Nano 9 (2015) 2635–2647.
[74] N. Lu, J.G. Wang, S.F. Xie, J. Brink, M. Mavrikakis, Y.N. Xia, M.J. Kim, J. Phys. Chem. C 118 (2014) 28876–28882.
[75] L. Zhang, L.T. Roling, X. Wang, M. Vara, M.F. Chi, J.Y. Liu, S.I. Choi, J.H. Park, J.A. Herron, Z.X. Xie, M. Mavrikakis, Y.N. Xia, Science 349 (2015) 412–416.
[76] X.H. Xia, L.F. Cosme, J. Tao, H.C. Peng, G.D. Niu, Y.M. Zhu, Y.N. Xia, J. Am. Chem. Soc. 136 (2014) 10878–10881.
[77] Q.C. Feng, S. Zhao, D.S. He, S.B. Tian, L. Gu, X.D. Wen, C. Chen, Q. Peng, D.S. Wang, Y.D. Li, J. Am. Chem. Soc. 140 (2018) 2773–2776.
[78] J.J. Ge, D.S. He, W.X. Chen, H.X. Ju, H. Zhang, T.T. Chao, X.Q. Wang, R. You, Y. Lin, Y. Wang, J.F. Zhu, H. Li, B. Xiao, W.X. Huang, Y.E. Wu, X. Hong, Y.D. Li, J. Am. Chem. Soc. 138 (2016), 13850-1385.
[79] Z.C. Zhang, Y. Liu, B. Chen, Y. Gong, L. Gu, Z.X. Fan, N.L. Yang, Z.C. Lai, Y. Chen, J. Wang, Y. Huang, M. Sindoro, W.X. Niu, B. Li, Y. Zong, Y.H. Yang, X. Huang, F.W. Huo, W. Huang, H. Zhang, Adv. Mater. 28 (2016) 10282–10286.
[80] L.Z. Bu, N. Zhang, S.J. Guo, X. Zhang, J. Li, J.L. Yao, T. Wu, G. Lu, J.Y. Ma, D. Su, X.Q. Huang, Science 354 (2016) 1410–1414.
[81] J.J. Ge, D.S. He, L. Bai, R. You, H.Y. Lu, Y. Lin, C.L. Tan, Y.B. Kang, B. Xiao, Y.E. Wu, Z.X. Deng, W.X. Huang, H. Zhang, X. Hong, Y.D. Li, J. Am. Chem. Soc. 137 (2015) 14566–14569.
[82] P.N. Duchesne, Z.Y. Li, C.P. Deming, V. Fung, X.J. Zhao, J. Yuan, T. Regier, A. Aldalbahi, Z. Almarhoon, S.W. Chen, D.E. Jiang, N.F. Zheng, P. Zhang, Nat. Mater. 17 (2018) 1033–1039.
[83] Y.H. Peng, Z.G. Geng, S.T. Zhao, L.B. Wang, H.L. Li, X. Wang, X.S. Zheng, J.F. Zhu, Z.Y. Li, R. Si, J. Zeng, Nano Lett. 18 (2018) 3785–3791.
[84] G. Kyriakou, M.B. Boucher, A.D. Jewell, E.A. Lewis, T.J. Lawton, A.E. Baber, H.L. Tierney, M.F. Stephanopoulos, E.C. Sykes, Science 335 (2012) 1209–1212.
[85] F.R. Lucci, J.L. Liu, M.D. Marcinkowski, M. Yang, L.F. Allard, M.F. Stephanopoulos, E.C. Sykes, Nat. Commun. 6 (2015) 8550–8558.
[86] R. Long, Y. Li, Y. Liu, S.M. Chen, X.S. Zheng, C. Gao, C.H. He, N.S. Chen, Z.M. Qi, L. Song, J. Jiang, J.F. Zhu, Y.J. Xiong, J. Am. Chem. Soc. 139 (2017) 4486–4492.
[87] H.W. Huang, K. Li, Z. Chen, L.H. Luo, Y.Q. Gu, D.Y. Zhang, C. Ma, R. Si, J.L. Yang, Z.M. Peng, J. Zeng, J. Am. Chem. Soc. 139 (2017) 8152–8159.
[88] J.J. Mao, C.T. He, J.J. Pei, W.X. Chen, D.S. He, Y.Q. He, Z.B. Zhuang, C. Chen, Q. Peng, D.S. Wang, Y.D. Li, Nat. Commun. 9 (2018) 4958–4966.
[89] T.T. Chao, X. Luo, W.X. Chen, B. Jiang, J.J. Ge, Y. Lin, G. Wu, X.Q. Wang, Y.M. Hu, Z.B. Zhuang, Y.E. Wu, X. Hong, Y.D. Li, Angew. Chem. Int. Ed. 129 (2017) 16263–16267.
[90] D.S. Wang, Q. Peng, Y.D. Li, Nano Res. 3 (2010) 574–580.
[91] D.S. Wang, Y.D. Li, Inorg. Chem. 50 (2011) 5196–5202.
[92] J.J. Mao, Y.X. Liu, Z. Chen, D.S. Wang, Y.D. Li, Chem. Commun. 50 (2014) 4588–4591.
[93] J.J. Mao, T. Cao, Y.J. Chen, Y.E. Wu, C. Chen, Q. Peng, D.S. Wang, Y.D. Li, Chem. Commun. 51 (2015) 15406–15409.
[94] Y.F. Chen, J.J. Mao, R.A. Shen, D.S. Wang, Q. Peng, Z.X. Yu, H.F. Guo, W. He, Nano Res. 10 (2017) 890–896.
[95] H.P. Rong, J.J. Mao, P.Y. Xin, D.S. He, Y.J. Chen, D.S. Wang, Z.Q. Niu, Y.E. Wu, Y.D. Li, Adv. Mater. 28 (2016) 2540–2546.
[96] J.B. Zhang, W.W. Xu, L. Xu, Q. Shao, X.Q. Huang, Chem. Mater. 30 (2018) 6338–6345.
[97] W. Chen, R. Yu, L.L. Li, A.N. Wang, Q. Peng, Y.D. Li, Angew. Chem. Int. Ed. 122 (2010) 2979–2983.
[98] X.X. Wang, S. Hwang, Y.T. Pan, K. Chen, Y.H. He, S. Karakalos, H.G. Zhang, J.S. Spendelow, D. Su, G. Wu, Nano Lett. 18 (2018) 4163–4171.
[99] M.Z. Hu, S. Zhao, S.J. Liu, C. Chen, W.X. Chen, Zhu W, C. Liang, W.C. Cheong, Wang Y, Y. Yu, Q. Peng, K.B. Zhou, J. Li, Y.D. Li, Adv. Mater. 30 (2018) 1801878–1801885.

Junjie Mao received his Ph.D. from Tsinghua University in 2016. After postdoctoral research at BUCT (Beijing University of Chemical Technology)-CWRU (Case Western Reserve University) International Joint Lab, he joined in Anhui Normal University in 2018. His research interests include energy materials and electrochemistry.

Jun Li completed her undergraduate study at Wanjiang College of Anhui Normal University in 2018. Currently, she is a graduate student at Anhui Normal University. Her current research interests include the synthesis and electrocatalytic properties of ultrathin nanomaterials.

Jiajing Pei is currently a PhD candidate in Beijing University of Chemical Technology. He received his bachelor's degree from North China Institute of Science & Technology (2014) and his Master's degree from Beijing University of Chemical Technology (2017). He is interested in noble metal-based nanocrystals and electrocatalytic applications.

Yan Liu received her Ph.D. from University of Science and Technology of China in 2018. She then joined the Department of Chemistry, Anhui Normal University. Her research interests focus on the employment of multi-scale modeling methods for electron kinetics in complex systems.

Dingsheng Wang received his BS degree in Department of Chemistry and Physics, University of Science and Technology of China in 2004, and his PhD degree in Department of Chemistry, Tsinghua University in 2009, with Acad. Yadong Li. He did his postdoctoral research in Department of Physics, Tsinghua University, with Acad. Shoushan Fan. He joined the faculty of Department of Chemistry, Tsinghua University in 2012.

Yadong Li received his BS degree from the Department of Chemistry, Anhui Normal University in 1986 and his PhD degree from the Department of Chemistry, University of Science and Technology of China in 1998, with Acad. Yitai Qian. He joined the faculty of the Department of Chemistry, Tsinghua University in 1999 as a full professor. His research interests are focused on the synthesis, assembly, structure and application exploration of nanomaterials